NASA DEVELOP National Program
Virginia – Langley

Summer 2024

Brazil Space Weather

Assessment of Space Weather Impact on Precision Agriculture Using the Global Navigation Satellite System in Brazilian Farms

DEVELOP Technical Report
August 9th, 2024

Jennifer Hall, Analytical Mechanics Associates (Project Lead)
Alyson Bergamini, Analytical Mechanics Associates
Ann Ehrlich, Analytical Mechanics Associates
Melissa Marquez, Analytical Mechanics Associates

Advisors:
Dr. Xia Cai, NASA Langley Research Center (Science Advisor)
Dr. Min-Yang Chou, Catholic University of America, NASA Goddard Space Flight Center (Science Advisor)
Jamie Favors, NASA Headquarters

Leads:
Marisa Smedsrud (Virginia – Langley)
Laramie Plott (Virginia – Langley)

1. Abstract

In Brazil, equatorial plasma bubbles (EPBs) are the primary space weather phenomenon impacting the performance of Global Navigation Satellite Systems (GNSS), causing signal disruptions and positional inaccuracies in agricultural machinery used for mapping fields, guiding equipment, and ensuring accurate planting, chemical application, and harvesting. As a result, farmers and stakeholders face challenges in maintaining accurate operational capabilities, often needing to shut down machinery to mitigate these effects. This project evaluates the feasibility of using NASA's Heliophysics observations for a case study in March 2024. Focusing on this month of observations narrows the perspective to align with the harvest season in Brazil, corresponding with a profitable, relevant time of the year. Data from NASA's Global-scale Observations of the Limb and Disk (GOLD) instrument is used to characterize EPBs, while amplitude and phase scintillation indices from ground-based GNSS receivers confirm their presence and impact on signal disruptions. Additionally, we assessed the practical implications of these disruptions on Real-Time Kinematic (RTK) GNSS-based operations using data from a local rover receiver to calculate the two-dimensional (2D) error and evaluate the impact on crop yield using harvest data. The project involved collaboration across multiple different organizations and sectors, including John Deere in Brazil for equipping agricultural tools with GNSS technology, Pamplona Farm owned by SLC Agrícola for data acquisition, and São Paulo University for data processing. The results aim to inform Brazilian farmers about position errors affecting their precision agriculture operations, formulate suggestions as to processing relevant data for the purpose of farming, and provide insights into the needs of space weather data users. Lessons from this case study will guide future integration of space weather data and modeling with end users.

Key Terms

precision agriculture, Global Navigation Satellite Systems (GNSS), ionospheric scintillation, equatorial plasma bubbles (EPBs)

2. Introduction

2.1 Background Information

Space weather encompasses solar and geomagnetic phenomena that can interfere with satellite infrastructure. These phenomena, including solar flares, geomagnetic storms, and ionospheric disturbances, disrupt communication and navigation systems, power grids, and other critical space-based functions. Modern Global Navigation Satellite Systems (GNSS), including the United States-based Global Positioning Systems (GPS) have algorithms to correct for normal levels of scintillation (refractions in signal) caused by space weather events (Prol et al., 2017). Among ionospheric disturbances, equatorial plasma bubbles (EPBs) are of concern due to their disruption of radio signals, affecting GNSS and GPS, as well as other satellite-based communications (Chu et al., 2005). EPBs are large-scale ionospheric irregularities that cause significant levels of scintillation in GNSS signals and develop near the geomagnetic equator after dusk. EPBs are regions of low plasma density that form in elongated structures, particularly influenced by the Rayleigh-Taylor instability, which describes the unstable interface where a lower density fluid pushes upward into a higher density fluid (Kelley et al., 1976). However, anticipating EPB occurrences and understanding the evolution in space and time remain active research areas (Sousasantos et al., 2024).

Disruptions in satellite signals caused by EPBs adversely affect the accuracy of GNSS positioning in countries around the geomagnetic equator, leading to inefficiencies and losses in agricultural productivity (Wiese, 2024). Precision agriculture relies heavily on these satellite-based systems to optimize farming practices. Farms collect large amounts of data regarding moisture, soil health, and crop yield from sensors in the field and attached to their equipment. To enhance farmer's decision-making according to the spatial variability of these factors, the data must be georeferenced with high accuracy and precision. GNSS-equipped vehicles and machinery also rely on GNSS during operation in the fields. While access to these data allows for the precise application of inputs and maximized efficiency during key farming operations like planting and harvesting, disruptions or errors in positioning can lead to overlapping or missed areas, negatively impacting crop yield and resource use efficiency (Perez-Ruiz & Upadhyaya, 2012).

Brazil's location along the geomagnetic equator makes it particularly relevant to our team's study of space weather effects on agriculture. This area of the world experiences a reduction in electron density at the equator and higher densities to the north and south, known as the equatorial ionization anomaly; this structure leads to strong ionospheric scintillations over Brazil (Chu et al., 2005; Spogli et al., 2013). Previous studies in Brazil have demonstrated that GPS signals experience greater disruption from scintillation when progradation paths coincide with EPBs (Moraes et al., 2018). De Paula et al. (2003) investigated the impacts of the equatorial ionization anomaly on GNSS signals in Brazil and found that the scintillation index (S4) is lower around the magnetic equator and higher near the equatorial anomaly crest. However, despite the likelihood of ionospheric interference, many Brazilian farmers continue to utilize precision farming technologies for efficient sowing and harvesting (Wiese, 2024). In 2022, the Brazilian government launched Law No. 14.475, which promotes the adoption of precision agriculture and expansion of use across Brazil by offering potential "financial incentives or subsidies" (Lei No. 14.475). This legislative support has made Brazil a favorable business environment for the precision agriculture industry, with MarkNtel Advisors estimating an increase of 18% in compound annual growth rate in the Brazilian precision agriculture market during the 2024 – 30 period (MarkNtel Advisors, 2024).

To lessen the impact of the nightly GNSS disruptions caused by plasma bubbles, some Brazilian farmers operate their machines according to strict operating windows when they predict scintillation will be minimal, from 4 AM to 8 PM. The loss of potential operating time for GNSS equipment has several implications for harvest operations: firstly, delays in harvest mean that crops must remain in the field beyond the optimal growth stage for harvesting; secondly, crops could be exposed to additional precipitation or moisture that affect the efficiency of future harvesting; finally, harvest delays put the remainder of the field left uncollected at risk of extreme weather, pests, or other events that could destroy some or all of the remaining crop yield. While none of these impacts are guaranteed, the risk of massive losses of potential yield means that more effective strategies to avoid positioning errors caused by plasma bubbles should be implemented.

2.2 Project Partners

While the results from this project can inform precision agriculture in Brazil more broadly, we performed this feasibility study primarily for Companhia Nacional de Abastecimento (CONAB), a public corporation that plays a crucial role in Brazil's agricultural sector by monitoring supply and demand, estimating crop yields, stabilizing prices, managing public food stocks, and supporting family farming (CONAB, n.d.). Traditionally, yield estimation in Brazil has been based on field measurements at farms; however, in recent years, Brazilian farms increased the use of GNSS-related technology for convenience and accuracy. Therefore, this study is important to CONAB as it evaluates the feasibility of using GNSS data to improve the efficiency of their yield estimation processes, as CONAB's crop yield estimation is crucial for providing accurate harvest projections to Brazil's Ministry of Agriculture and ensuring the financial security of local farms.

In addition to the main end user, we also had several collaborators for this project. The first of these is SLC Agrícola, one of Brazil's largest agricultural producers which integrates advanced technologies into farming practices to enhance efficiency and productivity. Operating 22 farms across six states, SLC Agrícola produces soybeans, corn, and cotton, among other crops (SLC Agrícola RI, 2023). SLC Agrícola enhances their agricultural practices using industry-leading precision agriculture technology provided by John Deere. Their equipment uses John Deere's StarFire Real-Time Kinematic (RTK) 7000 receivers, which provide high-accuracy correction signals, supporting GNSS constellations (GPS, GLObalnaya NAvigatsionnaya Sputnikovaya Sistem [GLONASS], Galileo, and BeiDou) with precision down to a few centimeters. Despite these capabilities, position errors still occur due to signal obstructions and ionospheric disturbances. To assist in this project, SLC Agrícola provided data from one of their farms, Pamplona. We used data from a corn field of this farm to help quantify operational times, specifically the curfew recommended by John Deere.

Because of their close connection to SLC Agrícola, we also worked with John Deere in Brazil. They provide farming technology to SLC Agrícola including sensors, machines, and an online platform to aggregate and

analyze data from precision agriculture operations. However, the value of these products is dependent on the accuracy of GNSS signals to their receivers, which are degraded by the occurrence of EPBs. To mitigate these effects, John Deere advises SLC Agrícola and other agri-businesses to turn off machinery at sunset when scintillation is most severe, preventing significant errors during critical operations like planting and harvesting. Our quantification of operational times leading to financial and temporal waste can potentially educate John Deere and their clients about the impacts of space weather.

We connected with São Paolo State University located in Presidente Prudente (UNESP). During the data acquisition process from the Ionospheric Scintillation Monitoring Receivers (ISMR) tool, Dr. Joao Francisco Galera Monico from UNESP reached out and joined our project to provide knowledge of GNSS and the interaction with moving machinery accomplished by the Study Group on Space Geodesy, or Grupo de Estudo em Geodésia Espacial. Their purpose is to mitigate the impacts of ionospheric disturbances on technology, and they achieve this by using several frequencies and receivers to combine information and reduce error. They modify their models to specify data and visualize it in a way that assists with flight navigation, deformation monitoring, and precision agriculture. Dr. Joao Francisco Galera Monico and Brian Leite Machado provided guidance on data processing.

2.3 Objectives and Study Area

With this project, we aimed to assist agricultural businesses and organizations, such as CONAB, John Deere, and SLC Agrícola, by demonstrating the feasibility of characterizing space weather threats to farming practices, estimating positioning errors, and developing strategies to optimize efficiency in responses to ionospheric disturbances. Additionally, this project builds capacity by increasing awareness among farmers and land managers about space weather phenomena and their impacts. We addressed often-overlooked challenges, improving farmers' awareness regarding resource allocation, planting schedules, and farm rover curfews. Farmers' and agri-business' understanding of GNSS positioning errors has the potential to lower inaccuracies, and results from this project can inform future projects on how to reduce errors.

To explore EPB phenomena over Brazil and globally, we utilized Earth observation data to characterize EPBs focusing on the seven states where SLC Agrícola operates farms (Figure 1). The study concentrated on two specific 48-hour periods: March 1 – 2, 2024, with high solar activity and plasma bubbles, and March 24 – 25, 2024, with weak solar activity and no evidence of plasma bubbles. This selection allowed us to visually capture the effects of different solar conditions on EPBs and their possible impact on GNSS signals. Our project leverages NASA's Global-scale Observations of the Limb and Disk (GOLD) on the SES-14 satellite to determine the feasibility of using NASA data to characterize the spatiotemporal features of EPBs over Brazil and on a global scale. We completed this project to validate the GOLD data by utilizing the European Space Agency's Electric Field Instrument aboard the Swarm Magnetic Field Mission. Furthermore, we aimed to use data from rovers and ground-based receivers to identify two-dimensional (2D) GNSS errors over Brazil and quantify the uncertainty in crop yield estimations affected by scintillation.

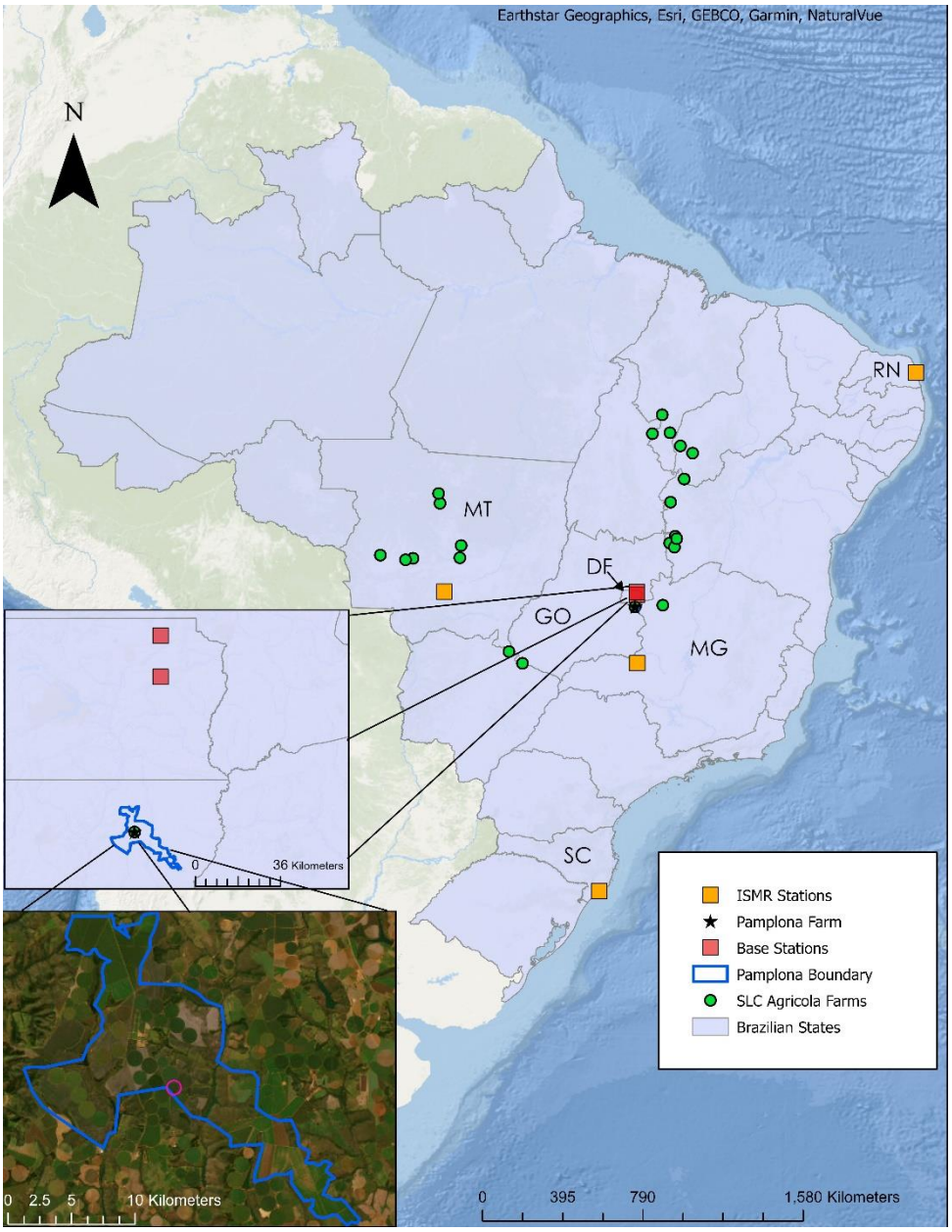

Figure 1. Map of farm locations managed by SLC Agrícola.

3. Methodology

3.1 Data Acquisition

3.1.1 Spatiotemporal Features of EPBs

GOLD Data

We obtained data from NASA's GOLD mission for March 1 – 2 and 24 – 25, 2024. GOLD, aboard the SES-14 satellite deployed in 2018, provides far-ultraviolet imaging of the ionosphere (Eastes et al., 2020). These Level 2 data, received as a Network Common Data Form (NetCDF) through the GOLD database, captured the ionosphere from two channels, each covering one hemisphere.

Rate of Total Electron Content Index (ROTI)

To characterize EPBs at a global scale, we accessed the Institute for Space-Earth Environmental Research (ISEE) database containing Rate of Total Electron Content index (ROTI) data. The 2D global total electron

content data in the ISEE database comes from GNSS observation data in Receiver Independent Exchange (RINEX) format, collected from a network of over 8,800 regional GNSS receivers worldwide, unlike GOLD data which comes from a single Earth observation mission (Table A1). ROTI is a common and widely used ionospheric disturbance index and often correlated to EPBs (Buhari et al., 2017; Nishioka et al., 2008). It is defined as the standard deviation of the rate of total electron content over a specific time interval along the satellite-receiver path, depicting EPBs as drastic depletions in electron content and density (Pi et al., 1997).

3.1.2 GNSS Error

ISMR GNSS Stations

There are currently several networks of ionospheric monitoring ground stations across Brazil providing spatial and temporal coverage. These networks provide data for parameters such as the intensity of phase and amplitude scintillation of the signals received by each station, the satellite that sent the signal, and total electron content (De Paula et al., 2023). Data from several of these networks is accessible via the ISMR Query Tool, a web interface designed for visualization and analysis of scintillation indices and related signal metrics (Vani et al., 2017). The tool provided access to monitoring data, aiding in our understanding of GNSS signal degradation. Ground station data can be accessed through the Brazilian Network for Continuous Monitoring of the GNSS Systems website and ISMR Query Tool website. GNSS data can be downloaded from the UNESP affiliate website (Group on Space Geodesy, 2014). The Group on Space Geodesy, developed this tool to monitor the ionosphere for the Concept for Ionospheric Scintillation Mitigation for Professional GNSS in Latin America (CIGALA) and Countering GNSS High Accuracy Applications Limitations due to Ionospheric Disturbances in Brazil (CALIBRA) projects. We acquired station reports of the S4 and sigma phi indices, which characterize the amplitude and phase scintillation of the signal respectively, from March 1 until March 31, 2024, at four different ground stations in Brazil: STMC, in the center of the country; STNT, on the easternmost shore; STCB, further west in the state of Mato Grosso; and STBR, in the south (Figure 1).

Pamplona Farm Receivers

John Deere provided RINEX format data for both rover and base stations for the study dates (March 1 – 2) at Pamplona Farm, including mixed observation data from multiple GNSS constellations and navigation messages for GPS, Galileo, and GLONASS satellite systems. These data encompassed RTK rover with corresponding base station data, and receiver using Precise Point Positioning. SLC Agrícola rovers use reference stations located over 30 kilometers away and employ a proprietary geostationary satellite that provides precise satellite data to correct positioning errors for Precise Point Positioning.

3.1.3 Productivity Impact

Operating Window

We used information from SLC Agrícola regarding their use of a standard operating window for their machines to avoid scintillation in the evenings caused by EPBs: 8 PM – 4 AM Brasilia Time (BRT). We downloaded data from the STMC ISMR station, located in the center of the country near Brasilia, for the entire month of March 2024 from the ISMR query tool. We converted the data to BRT, which is three hours behind Coordinated Universal Time (UTC).

Field Reports

SLC Agrícola also contributed field report data from one corn field in Pamplona Farm, just south of Brasilia. Pamplona Farm is a corporate agricultural area owned and operated by SLC Agrícola. This report contained data from 12 working hours over three days of harvest operations from July 2 – 4, 2024. It contained data regarding crop yield in dry matter and other specifications.

3.2 Data Processing and Visualization

3.2.1 Spatiotemporal Features of EPBs

GOLD Data

We utilized Python version 3.11 through Google Colab to characterize EPBs by analyzing radiance values from GOLD data. GOLD measures the radiance of far ultraviolet light from Earth's upper atmosphere, including the themosphere and ionophsere. In this case, we analyzed 135.6 nm, the ultraviolet wavelength of emissions gathered by GOLD in the ionosphere. We could identify EPBs by their nighttime ionospheric emission by atomic oxygen OI 135.6 nm radiance wave type (Eastes et al., 2017). We examined the radiance category defined in the GOLD NetCDF file. To create a chart showing the correlation between this variable and latitude, we installed five libraries in Python: Geopandas (ver. 1.0.0), NetCDF4 (ver.1.7.1.post1), OSMnx 1.9.4, the Climate Data Store API (ver. 0.7.2), and Libspatialindex-dev (ver 2.0.0). To show the correlation between radiance and latitude, we joined and transposed the March 1 – 2 files, ensuring correct variable formatting. We then filtered the data for the relevant period and latitudes, and we created line charts of radiance for March 1 – 2 and March 24 – 25. We also mapped these parameters using Cartopy. With the Cartopy Nearside Perspective projection, we positioned the data over Brazil and created scatterplots with colormaps for radiance values. We used gridlines and a global view to present points for the evenings of March 1 and 24 using the plate carrée projection.

ROTI

We imported ROTI data, available as NetCDFs in 10-minute intervals since 1993, using Cartopy and Xarray. We selected specific UTC times, converted them to integers, defined a color bar, and presented the data on global maps for the evenings of March 1 and 24, 2024 (Figure J1). We also set this ROTI data as the basemap in ArcGIS Pro version 3.3.0 and fit to the plate carrée projection, then overlaid data from four ISMR ground stations: STMC, STNT, STBR, and STCB. We pinpointed these stations with triangular markers. The S4 index value, representing the amplitude scintillation, determined the shade of color, and the sigma phi value, the quantification of signal strength, determined the size of the marker.

Ionospheric Bubble Probability (IBP) Model

To complement the radiance and ROTI data, we utilized the ionospheric bubble probability (IBP) model v1.2.1 (Stolle et al., 2024) to predict the occurrence probability of EPBs. The model incorporates empirical data from the Swarm satellite missions using the Electric Field Instrument to provide a statistical output characterizing the probability of low latitude bubble occurrence based on parameters such as the day of the year, longitude, local time, and the F10.7 cm Solar Flux index (f107). This index measured solar radio emissions at a wavelength of 10.7 cm, which is a proxy for solar activity. Higher values typically indicate more active solar conditions, which can enhance ionospheric disturbances. Ibp (2024) on GitLab contained the python code and documentation available. We used this code to map IBP by first installing the ibpmodel library, calculating the index for the day, time, and location of our focus, highlighting which solar flux dimension we are interested in, and plotting charts (Figures C1, C2, and C3). We used the plotIBPindex tool and plotButterflyData function to generate our graphics for March 1, March 24, and all of 2024.

3.2.2 GNSS Error

Pamplona Farm Receivers

We processed the RINEX format files from rover named 100633 and reference station named 100152, along with Precise Point Positioning receiver 100626 used at Pamplona Farm in RTKlib. RTKlib is an open-source software package for precise GNSS positioning and offers tools for converting, analyzing, and visualizing GNSS data. It includes a portable program library and several applications that leverage this library. One of the applications we used is RTKPost to generate position files. We uploaded the rover and base data in static mode with specific configurations to generate the final easting and northing values used as estimated position reference coordinates (Figure D1). Brian Machado and Dr. Joao Francisco Galera Monico processed the RINEX files and provided screenshots of the configuration settings (Figures D1, E1). We used the coordinates to compute positional differences and 2D errors for both receivers 100633 and 100626 using Excel.

ISMR GNSS Stations

For the scintillation indices, we used Python version 3.1.1 in Google Colab to process the ISMR data. We filtered the data from the STMC station on March 1 – 2 and March 24 – 25 to only include signals from GPS satellites at elevation angles greater than 10°. We converted the timestamps for each signal to datetime objects, and the S4 and sigma phi values were converted to numerical values. We grouped the signals by minute, and the maximum scintillation value for each minute was identified. Then, we visualized these values in a scatter plot, with each point color-coded according to which GPS satellite the maximum S4 value came from (Figures G1, G2, G3, G4).

3.2.3 Productivity Impact

Operating Window

For the March STMC data, we used the same processing as for the scintillation indices to identify the maximum S4 values per minute from GPS satellites, with the only change being that the data was filtered by an elevation angle of 15° instead of 10° to avoid highlighting error caused by satellites at low angles. We also converted the timestamp of each signal to BRT. We used the threshold of moderate scintillations (S4 > 0.5) to quantify the stretches of available work time that avoided EPBs (Figures H1, I1).

Field Reports

We used the yield mass values, measured in tons per hectare, converted by multiplying it by the dividend of the area of the crop circle and the number of harvesting points gathered. Next, we converted these yield masses for each point to the actual dry matter weight by multiplying each value by its corresponding dry matter percentage. We totaled each observation and divided it by the 12-hour span for which the machines were harvesting. We found the tons of corn harvested per hour, multiplied by the average delayed hours of work opportunity per day in March 2024, to estimate the tons of corn at risk from delaying harvesting in that field. That value, multiplied by the price of corn according to the United States Department of Agriculture's 2024 report, quantified the delayed harvest of corn put at risk of degradation or harm from natural causes (United States Department of Agriculture Foreign Agricultural Service, 2024).

3.3 Data Analysis

3.3.1 Spatiotemporal Features of EPBs

GOLD

We visualized nighttime radiance over Brazil for March 1 – 2 and March 24 – 25, comparing it to Swarm Electric Field Instrument data to validate the probability of nighttime EPBs. Additionally, we created global ROTI maps to monitor ionospheric irregularities, providing a broader context for understanding the spatial and temporal distribution of EPBs. We presented a qualitative relationship between ionospheric density depletions and severe scintillation values of S4 and sigma phi.

3.3.2 GNSS Error

ISMR GNSS Stations

To evaluate the positional discrepancies between measured and reference coordinates, we calculated the east and north components of the baseline errors in Excel, denoted as DE and DN respectively . We obtained the DE value by subtracting the reference easting value (eref) from the measured easting value (e-baseline). Similarly, we calculated DN by subtracting the reference northing value (nref) from the measured northing value (n-baseline). To quantify the magnitude of these errors, we squared the differences to obtain DE^2 and DN^2. These squared values represent the variance in the easting and northing directions. Finally, we computed the overall horizontal error, or 2D error, by taking the square root of the sum of DE^2 and DN^2. While vertical accuracy (part of 3D error) is also important, it is less critical for the specific task of following guidance lines during harvesting operations. This 2D error measured positional accuracy by combining easting and northing errors into a single value, representing the Euclidean distance between the measured and reference positions in the horizontal plane.

Pamplona Farm Receivers

We set thresholds to identify when maximum S4 and maximum sigma phi reached moderate and severe levels. For S4, a value of 0.5 indicated moderate amplitude scintillation, while values of 0.8 or greater corresponded with severe amplitude scintillation (De Paula et al., 2023). For sigma phi, a threshold of 0.4 indicated low phase scintillation, and we associated 0.7 or above with severe phase scintillation (Aquino et al., 2009). We then extracted these values and ROTI values from 8 PM – 12 AM BRT over Brazil into a CSV file and created a map in ArcGIS Pro version 3.3.0. The thresholds helped perceive the magnitude of scintillation over the GNSS stations and correlate it with ROTI values depicted as pixels in the background. We also compared these values to the 2D error from the receivers at Pamplona Farm.

3.3.3 Productivity Impact

Operating Window

To quantify the impact of ionospheric scintillation caused by EPBs on the productivity of precision agriculture, we identified the potential operating window for GNSS operations at STMC station for each day in the month of March 2024 (Figure H1). We defined the beginning of the potential operating window as the last instance of scintillation above the moderate threshold for S4 before noon; and the end of the window as the first occurrence after noon. We then subtracted the standard operating window from the new potential operating window to get the difference in time for each day (Figure I1). Finally, we summed up the additional hours outside of the standard window for the entire month and calculated the average.

4. Results & Discussion

4.1 Analysis of Results

4.1.1 Spatiotemporal Characterization using GOLD

We found radiance to be a useful characteristic to analyze for predicting ionospheric activity. With low radiance, photoionization could not occur, meaning plasma would not regenerate, thus leaving depressions available for bubbles to form. This is why EPBs formed at night, when solar intensity was negligible. The chart of radiance additionally provided assurance of a trough at Brazil's latitude (approximately 16°S) on March 1 – 2, while March 24 – 25 showed little potential for the formation of EPBs (Figure B1, B2). Total electron content tracked the density of the ionosphere. Depressions in these values suggest potential for bubbles to form, as seen along the geomagnetic equator on the evening of March 1 (Figure 2). The peak electron density in the upper ionosphere, known as NmF2, which GOLD collected as its Level 2 data product NMax, shows a nighttime trough when visualized at the latitude corresponding with Brazil, meaning it was a likely area for EPBs (Figure 3).

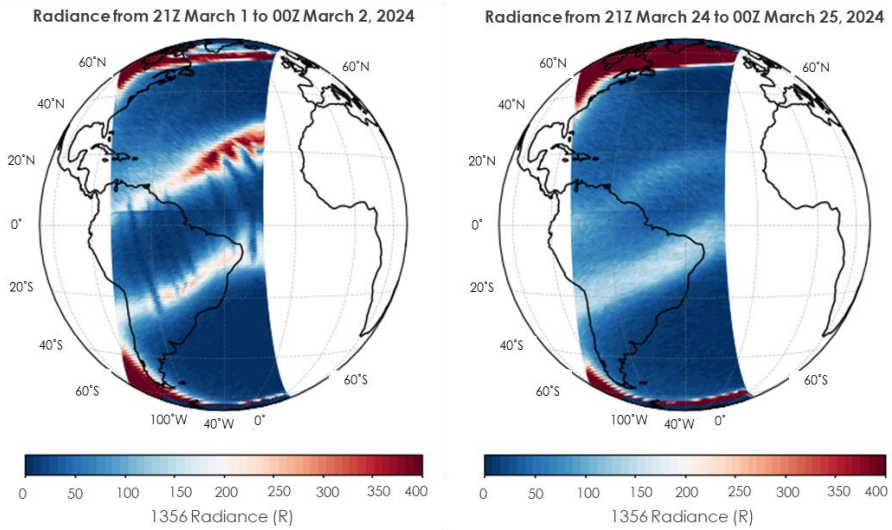

Figure 2. Global radiance map on March 1 (left) and March 24 (right)

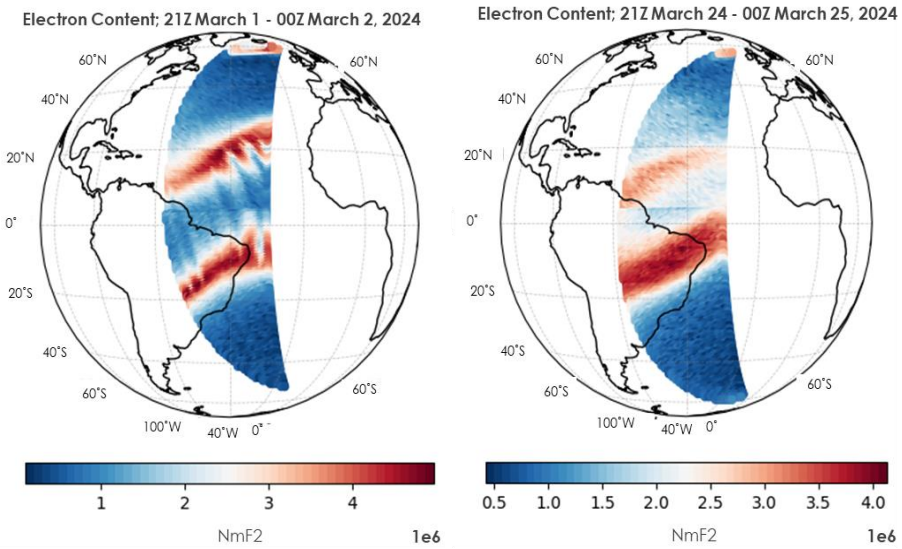

Figure 3. Global NMax (peak electron density in the upper ionosphere, or NmF2) map on March 1 (left) and March 24 (right)

4.1.2 Ionospheric Bubble Probability Model

The output of the IBP model demonstrates the peak potential at Brazil's longitude (approximately 47°W) during nighttime, when EPBs are most often impactful (Figure C1). This is evident from the high probability (about 80%) region shown in the plot (Figure C1), indicating that the likelihood of ionospheric bubbles is greatest around 10 PM. The 10.7cm radio flux for March 1 was 150.1 s.f.u. or 10 – 22 W m^{-2} Hz^{-1} and daily indices can be determined through https://omniweb.gsfc.nasa.gov/form/dx1.html. This model predicted ionospheric activity on this evening. We also identified increased radio flux on the evening of March 24 (Figure C2); however, EPBs did not form, suggesting they are a culmination of other factors. An increased IBP did not consider other factors, such as ROTI or radiance, which limited its accuracy. We looked at data for the entire year and found that distinct regions with high probabilities of ionospheric bubbles centered around -50°, decreasing past 0° longitude. The likelihood of EPBs is higher during the months of October to April, ranging from 50 – 65%, aligning with the active agricultural season in Brazil (Figure C3). These visualizations and charts supported the feasibility of identifying EPBs in more susceptible times of the year and day but do not provide a reliable method of prediction.

4.1.3 ROTI and ISMR Scintillation Correlation

We analyzed the evening of March 1 as an example of prevalent scintillations because of the higher ROTI values we identified for that evening versus March 24 (Figure J1). We noted a greater qualitative relationship between S4, signal strength, and sigma phi, signal timing, in response to ROTI. This index varied throughout the evening of March 1, 2024 (Figure 4). At 8 PM, we observed notable scintillations near the STNT station with high S4 and sigma phi values of 0.726 and 0.666, respectively, and a rapid density depletion indicated by a high ROTI value of 5.423. At 10 PM, these density depletions expanded deeper into Brazil, resulting in stronger scintillations at the STMC and STCB stations. However, even until 12 AM, the southernmost STBR station experienced negligible density depletions and weak scintillations as a result.

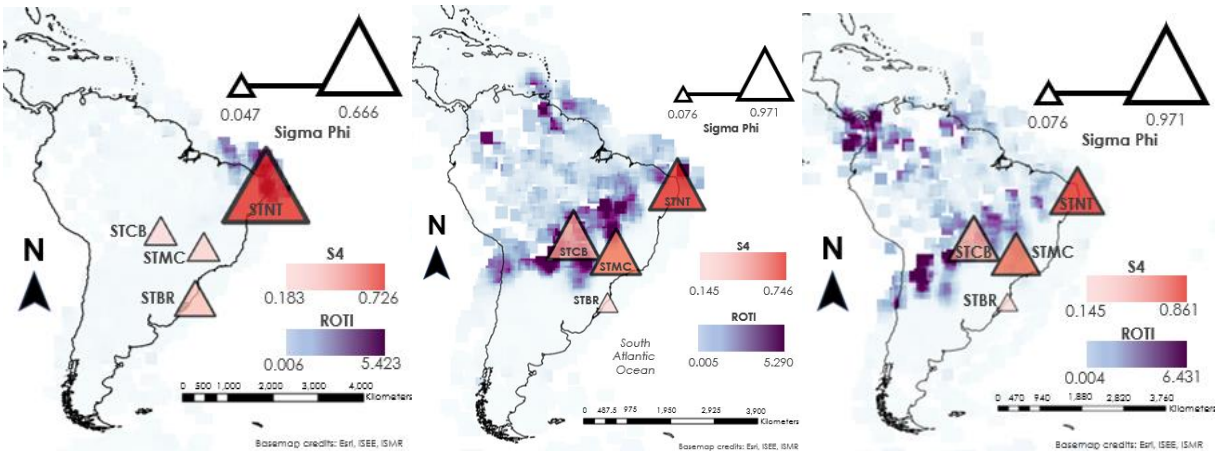

Figure 4. Qualitative relationship between S4, sigma phi, and ROTI values at Brazilian ground stations.

4.1.4 Pamplona Farm Receiver 2D Error

After calculating the 2D error from the position files described in section 3.2.3, we plotted the data comparing RTK rover 100633 and base receiver 100152 to Precise Point Positioning 100626 for the evening of March 1 into the early morning of March 2. It should be noted that the RTK rover and Precise Point Positioning were not in use this evening, as SLC Agrícola switches off their rovers. This analysis was to observe the effects of the scintillations on both correction techniques. Scintillations start to affect the 2D error of the RTK rover 100633 and reference base 100152 around 9 PM BRT and continue to vary up until 4 AM (Figure 5a). The effects of scintillations on Precise Point Positioning are noted around 10 PM BRT and last until 1 AM (Figure 5b). John Deere was unable to provide complete data for March 24 and 25; therefore, we plotted data for the evening of March 24 and found little to no scintillation effects on the 2D error for the Precise Point Positioning correction technique (Figure F1).

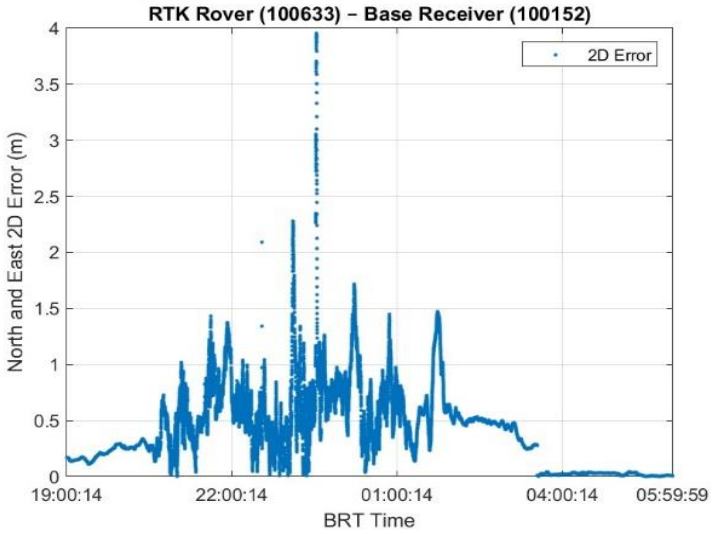

Figure 5a. 2D error seen on evening of March 1 into the early morning of March 2 on RTK correction technique

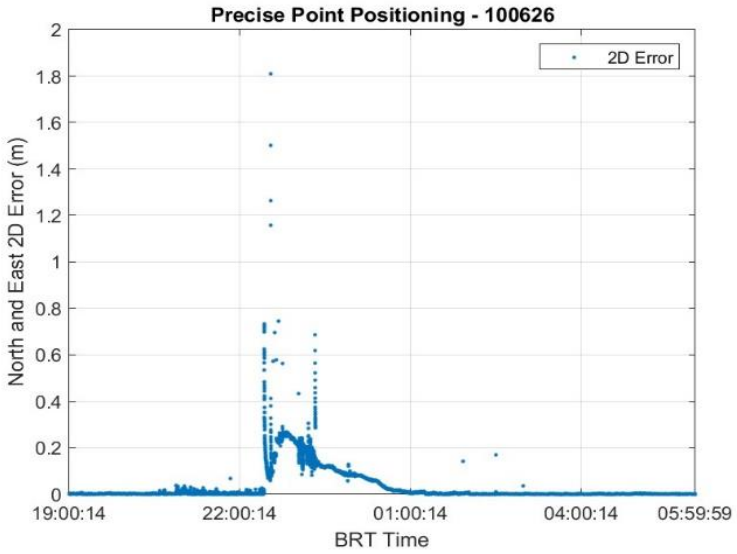

Figure 5b. 2D error seen on evening of March 1 into the early morning of March 2 on PPP correction technique

4.1.5 Precision Agriculture Productivity Impacts

As seen in the calendar in Figures H1 and I1, the standard operating window of 4 AM to 8 PM BRT does not reflect the actual potential operating window where ionosphere scintillation is below moderate levels. On average, farmers could have operated their GNSS-enabled machines an additional 4 hours and 27 minutes per day, for 138 hours and 9 minutes in March 2024. The only day where the calculated potential operating window was smaller than the standard was March 2, largely due to the plasma bubbles observed in the evening of March 1 lasting into the early morning hours. On March 24, when GOLD data observed no plasma bubbles, the potential operating window was the entire day. It should be noted that operating windows did get longer on average in the second half of the month compared to the first half of the month, validating the findings of the IBP model on the seasonal variability of EPBs.

In order to quantify the impact of an extra 4 hours and 27 minutes on agricultural operations, we first calculated from the field report that 576.09 tons of corn had been harvested from the crop field of study over 12 hours of machine operation, with only one machine operating at a time, meaning it harvested at a rate of 48.01 tons per hour. As such, not operating during the extra potential operating time outside of the standard window could have left 213.64 tons of corn that could have been harvested in the field for 8 hours until 4 AM the next day. According to the United States Department of Agriculture, Brazilian corn exports cost USD 285 per ton in late June 2024 (United States Department of Agriculture Foreign Agricultural Service, 2024), meaning the yield that could have been harvested was worth USD 60,888.68. Delays in harvesting, even only overnight, put the crop at risk of gradual degradation from remaining in the field past optimal harvesting conditions, inefficiency when harvest does occur due to increased moisture, and even potential loss of yield should extreme weather, pests, or other severe events occur.

4.2 Errors and Uncertainties

4.2.1 GOLD Data

GOLD data showed some inconsistencies when charting its values, overlapping along the equator. The GOLD imager scanned the Northern and Southern hemispheres separately, gathering two values for the same locations for 35° in latitude around the entire circumference of the Earth. This served as an example of calibration error and limited some of the accuracy of measurements for that area; however, the latitudes did not include those of Brazil. Additionally, GOLD nighttime observations ended just after midnight, limiting the available data. We noted the relevancy of this limit since EPBs were only impactful in the nighttime hours when photoionization was not occurring.

4.2.2 ISMR GNSS Data

Due to time constraints, we focused on the scintillation effects on L1 single frequency using only GPS satellites. GPS has three main signals: L1 (1575.42 MHz), L2 (1227.60 MHz), and L5 (1176.45 MHz). The ISMR Query Tool offers data for a variety of satellite constellations and frequency options. A previous study by Salles et al. (2021) demonstrated that the GPS L2C and L5 signals are more susceptible to scintillation effects. Thus, considering multiple constellations, such as Galileo and GLONASS, along with multiple frequency signals, could provide a more holistic understanding of the scintillation impacts. Scintillation effects from local temperature, humidity, and other variables in the lower atmosphere were also disregarded.

4.2.3 Ionospheric Bubble Probability Model

The IBP model has several constraints mentioned in Stolle et al. (2024) paper. The model estimates equatorial plasma depletion occurrence rates only at altitudes between 350 and 510 km and should not be used for solar flux indices F10.7 below 80 s.f.u. or above 200 s.f.u to avoid underestimating equatorial plasma depletion. Additionally, it only accounts for plasma depletions greater than approximately $2 \cdot 10^{11}$ m^{-3}. The model forecasts equatorial plasma depletion occurrence rates over specified longitudes and averaged across latitude. These constraints should be considered for any time-scale forecasting using IBP.

4.2.4 Precision Agriculture Productivity Impact

The benefits from utilizing the extra potential operating time outside of the standard window assumed that farmers could respond perfectly to changes in ionospheric conditions; much of the extra time each day is in the early morning after EPBs dissipate. However, scintillation can drop below moderate levels and spike back up multiple times in a night, so they cannot react immediately to the last instance of moderate scintillation. In addition, although we used corn harvest data from July 2 – 4, 2024, these data do not align with the periods of strong or weak scintillations that were analyzed in our study. Additionally, the estimated crop weight and price could vary seasonally in Brazil and due to other factors, such as weather and maintenance. This means more generalized estimations, including the hourly yield and hours of wasted available work time, likely have calculation errors.

4.3 Discussion of Results

We used multiple data sources to understand and visualize the ionospheric scintillations and their impact on GNSS errors in precision agriculture. We began by visualizing the IBP model, suggesting that March 1 and 24 of 2024 would be evenings experiencing strong solar fluxes. To confirm the likelihood of EPBs, we analyzed additional features from these evenings. Using GOLD data, we illustrated radiance and NMax values, which revealed that March 1 was an evening experiencing density depletions, while March 24 was not. By highlighting ROTI quantifications, we validated that there were notable density depletions only on March 1 in the evening. Using the S4 and sigma phi indices, we drew a correlation between density depletions from EPBs seen in ROTI data and amplitude and phase scintillations experienced at ground stations, thus impacting data used for precision agriculture in Brazil. Scintillation data were available for the STMC station, which was the nearest GNSS reference station to the Pamplona Farm. We concluded that when STMC had moderate scintillations on the L1 frequency signal, the receivers used at Pamplona Farm would have similar effects. While the 2D error seen on the RTK rover 100633 and Precise Point Positioning 100626 varied throughout the night, the start and end times of the displacement aligned with the beginning and end of nighttime scintillation caused by plasma bubbles (Figure G1).

The relationship between EPBs, ionospheric scintillation, and 2D positioning error supports curfews to avoid scintillation affecting the operation of their GNSS-enabled equipment. However, by validating the seasonal variability in EPB occurrence and duration shown by the IBP model with the variation in potential operating time through the month of March, we determined that these curfews can be adjusted based on the historic operating windows at different points in the growing season for each station.

4.4 Feasibility & Partner Implementation

Our partners can utilize our methods to inform their decision-making on when to operate equipment and how to account for the 2D error caused by plasma bubbles. Timelines for data availability, however, must be considered. While data from the ISMR Query tool becomes available within two weeks, GOLD data usually takes around one month to become available. This delay implies that real-time decision-making might be challenging. However, utilizing the IBP model can help in creating a calendar of operating hours and identify vulnerable days for future planning, as it simulates and predicts long-term ionospheric scintillation activity, capturing overall patterns and trends. As more Swarm observations become available, the model coefficients will be revised over time; thus, an annual update is projected. Methodology using previous working curfews to estimate extensions for working hours moving forward is an example of feasible time series forecasting that can be implemented by Brazilian farms.

GOLD, the ISMR Query Tool, and ISEE data can be downloaded for free; however, without prior knowledge or a deep dive into the literature review, it can be challenging to determine which specific data products to download. Even figuring out which software to use for opening or converting compressed files can be challenging. We believe that tutorials for downloading and processing GOLD and ISMR GNSS data would be highly beneficial for end users with no experience.

The RINEX files provided by John Deere are propriety, and it took a few weeks to obtain approval and receive the data. End users can download RTKlib and process raw rover and reference station data. The Group on Space Geodesy, from UNESP, and our science advisor Dr. Min-Yang provided substantial guidance. Although many tutorials are available online configuration settings are unique to each receiver and might require expert advice from GNSS specialists.

5. Conclusions

This study has provided valuable findings to Brazilian farmers, who could utilize similar methodologies moving forward to anticipate EPB presence. Using the IBP model, they could predict solar activity threats by day. The rover error quantifications validate the distortion in positioning caused by plasma bubbles that they experience when operating at night. Additionally, the calendar highlighting available work time could be replicated for other months from previous years to provide a proxy for upcoming harvesting seasons, since conditions rotate on a consistent solar calendar. It can also be replicated for other locations in Brazil to provide more tailored data for farms.

We found that multiple aspects of this study were feasible using remote sensing technology. It was feasible to visualize EBPs using ROTI data and GOLD's radiance observations for March of 2024. We validated GNSS positioning errors on these same dates with the visualized data from GOLD and ROTI. After confirming these positioning errors, we charted them to highlight hours within the focus dates where moderate to severe scintillation occurred. After identifying the hours of scintillation, we found that farms, such as those owned by SLC Agrícola, could expand operating times to optimize efficiency during this month. Expanding the operating times past the 16-hour window will maximize profit.

CONAB can use the data from this study to inform Brazilian farms about the effects of ionospheric scintillations on GNSS errors in precision agriculture. Greater awareness of ionospheric disturbances can help farmers make more informed decisions regarding GNSS-dependent equipment. We hope that our partners or Brazilian farmers will consider applying our methods to other months or seasons to maximize efficiency and profitability.

6. Acknowledgements

The Brazil Space Weather Team thanks our project partners from Companhia Nacional de Abastecimento (CONAB), SLC Agrícola, John Deere in Brazil, and São Paulo State University (UNESP). We are grateful to Dr. Xia Cai and Dr. Min-Yang Chou for advising this study, Jamie Favors for sponsoring DEVELOP's

collaboration with NASA Heliophysics Space Weather Program, and our DEVELOP Leads Marisa Smedsrud and Laramie Plott for offering guidance, support, and feedback throughout this project.

This material contains modified Swarm Electric Field Instrument data (2024), processed by ESA.
This material contains modified GOLD data (2024), processed by NASA.

Any opinions, findings, and conclusions or recommendations expressed in this material are those of the author(s) and do not necessarily reflect the views of the National Aeronautics and Space Administration.

This material is based upon work supported by NASA through contract 80LARC23FA024.

Global Navigation Satellite System – Total Electron Content (GNSS-TEC) data processing has been supported by JSPS KAKENHI Grant Number 16H06286. GNSS RINEX files for the GNSS-TEC processing are provided from many organizations listed by the webpage (http://stdb2.isee.nagoya-u.ac.jp/GPS/GPS-TEC/gnss_provider_list.html).

7. Glossary

CONAB – Companhia Nacional de Abastecimento, or in English, National Supply Company
EPB – Equatorial Plasma Bubble
Geomagnetic Equator – a line that connects all points on the Earth's surface where the magnetic field lines are parallel to the surface; does not align with the geographic equator, and runs directly over Brazil
GNSS – Global Navigation Satellite System
GOLD – Global-scale Observations of the Limb and Disk
GPS – Global Positioning System
Ground Stations – The GNSS stations studied around Brazil; STNT in Rio Grande do Norte, STCB in Mato Grosso, STMC in Minas Gerais, and STBR in Santa Catarina
IBP – Ionospheric Bubble Probability
ISEE – Institute for Space-Earth Environmental Research
ISMR Query Tool – Ionospheric Scintillation Monitoring Receivers Query Tool
NetCDF – Network Common Data Form
NMax – Peak electron density; derived from nightside disk images of OI 135.6 nm measurements
Pamplona Farm – Case study farm owned by SLC Agrícola
Precision Agriculture – Use of georeferenced data to guide agricultural operations
Radiance – Intensity of the energy captured by the sensor
Raleigh-Taylor Instability – Instability where a lighter fluid pushes a denser fluid
RINEX – Receiver Independent Exchange
ROTI – Rate of Total Electron Content Index
RTK – Real-Time Kinematic
S4 – Changes in signal strength as it travels between satellites and receivers
Scintillations – Irregularities in the ionosphere, may be affected by solar activity
Sigma Phi – Changes in signal timing as it travels between satellites and receivers
UNESP – São Paulo State University

8. References

Aquino, M., Monico, J. F., Dodson, A. H., Marques, H., De Franceschi, G., Alfonsi, L., Romano, V. & Andreotti, M. (2009). Improving the GNSS positioning stochastic model in the presence of ionospheric scintillation. *Journal of Geodesy*, *83*(10), 953–966. https://doi.org/10.1007/s00190-009-0313-6

Buhari, S. M., Abdullah, M., Yokoyama, T., Otsuka, Y., Nishioka, M., Hasbi, A. M., Bahari, S. A., & Tsugawa, T. (2017). Climatology of successive equatorial plasma bubbles observed by GPS ROTI over Malaysia. *Journal of Geophysical Research Space Physics*, *122*(2), 2174–2184. https://doi.org/10.1002/2016ja023202

Chu, F. D., Liu, J. Y., Takahashi, H., Sobral, A., Taylor, M. J., & Medeiros, A. F. (2005). The climatology of ionospheric plasma bubbles and irregularities over Brazil. *Annales Geophysicae*, *23*(2), 379–384. https://doi.org/10.5194/angeo-23-379-2005

CONAB. (n.d.). *National Supply Company CONAB*. Cooperacao Tecnica Brasileria Agricultura, Seguranca Alimentar e Pliticas Socialis. https://www.abc.gov.br/training/informacoes/InstituicaoCONAB_en.aspx

NASA. (2018). *Global-scale observation of the limb and disk* (Rev. 5.6) [Data set]. https://gold.cs.ucf.edu/data/search/

De Paula, E. R., Rodrigues, F. S., Iyer, K. N., Kantor, I. J., Abdu, M. A., Kintner, P. M., Ledvina, B. M., & Kil, H. (2003). Equatorial anomaly effects on GPS scintillations in Brazil. *Advances in Space Research*, *31*(3), 749–754. https://doi.org/10.1016/s0273-1177(03)00048-6

Eastes, R. W., McClintock, W. E., Burns, A. G., Anderson, D. N., Andersson, L., Codrescu, M., Correira, J. T., Daniell, R. E., England, S. L., Evans, J. S., Harvey, J., Krywonos, A., Lumpe, J. D., Richmond, A. D., Rusch, D. W., Siegmund, O., Solomon, S. C., Strickland, D. J., Woods, T. N., & Oberheide, J. (2017). The global-scale observations of the limb and disk (GOLD) mission. *Space Science Reviews*, *212*(1-2), 383–408. https://doi.org/10.1007/s11214-017-0392-2

Eastes, R. W., McClintock, W. E., Burns, A. G., Anderson, D. N., Andersson, L., Aryal, S., Budzien, S. A., Cai, X., Codrescu, M. V., Correira, J. T., Daniell, R. E., Dymond, K. F., England, S. L., Eparvier, F. G., Evans, J. S., Foroosh, H., Gan, Q., Greer, K. R., Karan, D. K., Krywonos, A., Laskar, I., Lumpe, J. D., Martinis, C. R., McPhate, J.B., Oberheide, J., Siegmund, O.H., Solomon, S. C., Veibel, V., & Woods, T. N. (2020). Initial observations by the Gold Mission. *Journal of Geophysical Research: Space Physics*, *125*(7). https://doi.org/10.1029/2020ja027823

Group on Space Geodesy. (2014). *ISMR query tool*. unesp. https://ismrquerytool.fct.unesp.br/is/ismrtool/manual/index.php

ibp. (2024). *IBP-Model* (Version 1.2.1) [Source Code] https://igit.iap-kborn.de/ibp/ibp-model

Kelley, M. C., Haerendel, G., Kappler, H., Valenzuela, A., Balsley, B. B., Carter, D. A., Ecklund, W. L., Carlson, C. W., Häusler, B., & Torbert, R. (1976). Evidence for a rayleigh-taylor type instability and upwelling of depleted density regions during equatorial spread F. *Geophysical Research Letters*, *3*(8), 448–450. https://doi.org/10.1029/gl003i008p00448

Lei No. 14.475, de 13 de Dezembro de 2022, FAOLEX Database, Março 2024 (Braz.). https://www.fao.org/faolex/results/details/en/c/LEX-FAOC213927

MarkNtel Advisors. (2024). *Brazil Precision Agriculture Market Research Report: Forecast (2024-2030).* https://www.marknteladvisors.com/research-library/brazil-precision-agriculture-market.html

Moraes, A. de, Vani, B. C., Costa, E., Abdu, M. A., de Paula, E. R., Sousasantos, J., Monico, J. F., Forte, B., de Siqueira Negreti, P. M., & Shimabukuro, M. H. (2018). GPS availability and positioning issues when the signal paths are aligned with Ionospheric Plasma bubbles. *GPS Solutions*, *22*(4). https://doi.org/10.1007/s10291-018-0760-8

Nishioka, M. & Saito, A. & Tsugawa, T. (2008). Occurrence characteristics of plasma bubble derived from global ground-based GPS receiver networks. *Journal of Geophysical Research 113*(A5). https://doi.org/10.1029/2007JA012605

Pi, X., Mannucci, A.J., Lindqwister, U.J. & Ho, C.M. (1997). Monitoring of global ionospheric irregularities using the worldwide GPS network. *Geophysical Research Letters, 24*(8). https://doi.org/10.1029/97GL02273

Perez-Ruiz, M. & Upadhyaya, S. K. (2012). GNSS in Precision Agricultural Operations. In F. Elbahhar & A. Rivenq (Eds.), *New Approach of Indoor and Outdoor Localization Systems*. IntechOpen. http://dx.doi.org/10.5772/50448

Prol, F. dos S., Camargo, P. de O., & Muella, M. T. de A. H. (2017). Comparative Study of Methods for Calculating Ionospheric Points and Describing the GNSS Signal Path. *Boletim De Ciências Geodésicas, 23*(4), 669–683. https://doi.org/10.1590/S1982-21702017000400044

Salles, L. A., Vani, B. C., Moraes, A., Costa, E., & de Paula, E. R. (2021). Investigating ionospheric scintillation effects on multifrequency GPS signals. *Surveys in Geophysics*, *42*(4), 999–1025. https://doi.org/10.1007/s10712-021-09643-7

Stolle, C., Siddiqui, T. A., Schreiter, L., Das, S. K., Rusch, I., Rother, M., & Doornbos, E. (2024). An empirical model of the occurrence rate of low latitude post-sunset plasma irregularities derived from Champ and swarm magnetic observations. *Space Weather*, *22*(6). https://doing.org/10.1029/2023sw003809

Sousasantos, J., Rodrigues, F. S., Gomez Socola, J., Pérez, C., Colvero, F., Martinis,C. R., & Wrasse, C. M. (2024). First observations of severe scintillation over low-to-mid latitudes driven by quiet-time extreme equatorial plasma bubbles: Conjugate measurements enabled by citizen science initiatives. *Journal of Geophysical Research: Space Physics*, *129*, e2024JA032545. https://doi.org/10.1029/2024JA032545

Spogli, L., Alfonsi, L., Romano, V., De Franceschi, G., Galera Monico, J. F., Shimabukuro, M. H., Bougard, B., & Aquino, M. (2013). Assessing the GNSS scintillation climate over Brazil under increasing solar activity. *Journal of Atmospheric and Solar-Terrestrial Physics*, *105-106*, 199-206. https://doi.org/10.1016/j.jastp.2013.10.003

United States Department of Agriculture Foreign Agricultural Service. (2024, August). *Grain: World Markets and Trade.* https://downloads.usda.library.cornell.edu/usda-esmis/files/zs25x844t/kw52m153h/kp78j760f/grain.pdf

Vani, B. C., Shimabukuro, M. H., & Galera Monico, J. F. (2017). Visual exploration and analysis of Ionospheric Scintillation Monitoring Data: The ISMR query tool. *Computers & Geosciences*, *104*, 125–134. https://doi.org/10.1016/j.cageo.2016.08.022

Wiese, H. (2024, February 20). THE CHALLENGE OF IONOSPHERIC SCINTILLATION IN PRECISION AGRICULTURE. *Association of Equipment Manufacturers*. https://www.aem.org/news/the-challenge-of-ionospheric-scintillation-in-precision-agriculture

9. Appendices

Appendix A: *Data Used for This Project*

Table A1
GOLD Far Ultraviolet Imager, ISEE Database, ISMR, Swarm, as they relate to this study

Dataset	Source	Parameter(s)	Use
GOLD Data	GOLD Far Ultraviolet Imager on SES-14	OI 135.6nm radiance; Level 2 - NMax	Identify EPBs over Brazil and monitor spatiotemporal evolution. Provide data on maximum ionospheric density values.
Global Navigation Satellite System – Total Electron Content (GNSS-TEC) Database	Space-Earth Environmental Research (ISEE), Nagoya University Database	Global ROTI Data (NetCDF)	Collect data on the change in TEC globally and over Brazil to be used for charting and mapping.
GNSS Stations: STMC, STNT, STBR, and STCB	ISMR Query Tool	Station Reports of S4 and sigma phi or σ Φ	Performs analysis on scintillation monitoring indexes from GNSS receivers in Brazil. Tracks S4 and sigma phi data daily.
L2 product	Electric Field Imager on Swarm Mission	Ionospheric Bubble Probability (IBP)	Determine probability of EPBs over Brazil with an hourly and monthly range correlating with longitude.
Raw receiver files	John Deere	Receiver data for RTK rover 100633 and base 100152, and PPP 100626	Analyze ground station data to visualize error. Data downloaded as Receiver Independent Exchange RINEX format
Corn harvest data	SLC Agrícola	Part of Pamplona Farm	Illustrate and analyze Pamplona Farm and its boundaries.

Appendix B: *GOLD Radiance Charts*

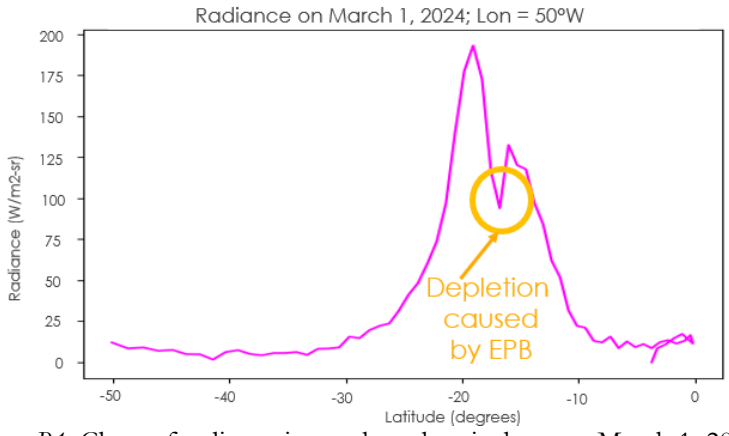

Figure B1. Chart of radiance in southern hemisphere on March 1, 2024

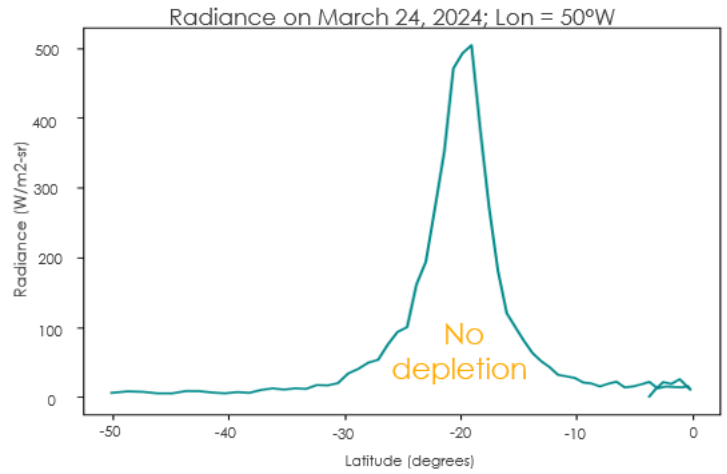

Figure B2. Chart of radiance in southern hemisphere on March 24, 2024

Appendix C: *IBP Model*

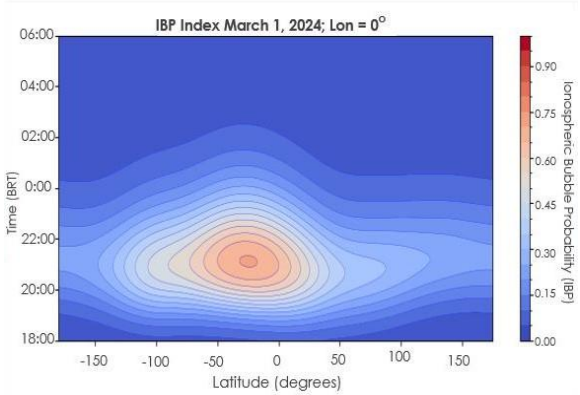

Figure C1. Map of IBP index for March 1, 2024

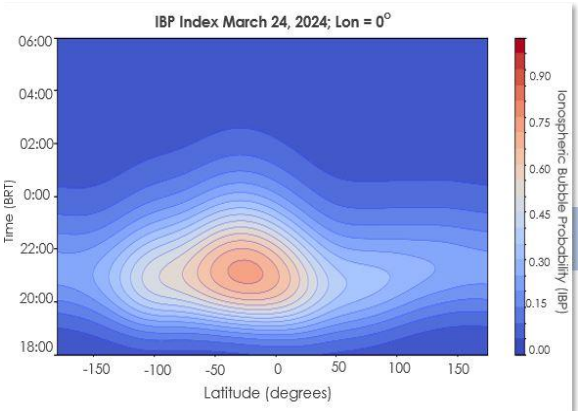

Figure C2. Map of IBP index for March 24, 2024

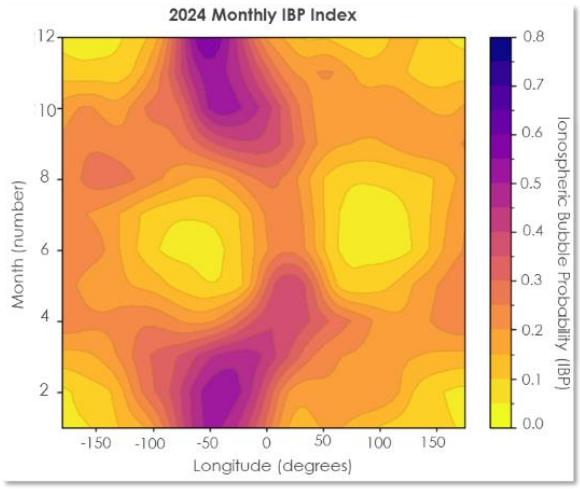

Figure C3. Heatmap of monthly IBP index through 2024

Appendix D: *Static Configuration Settings*

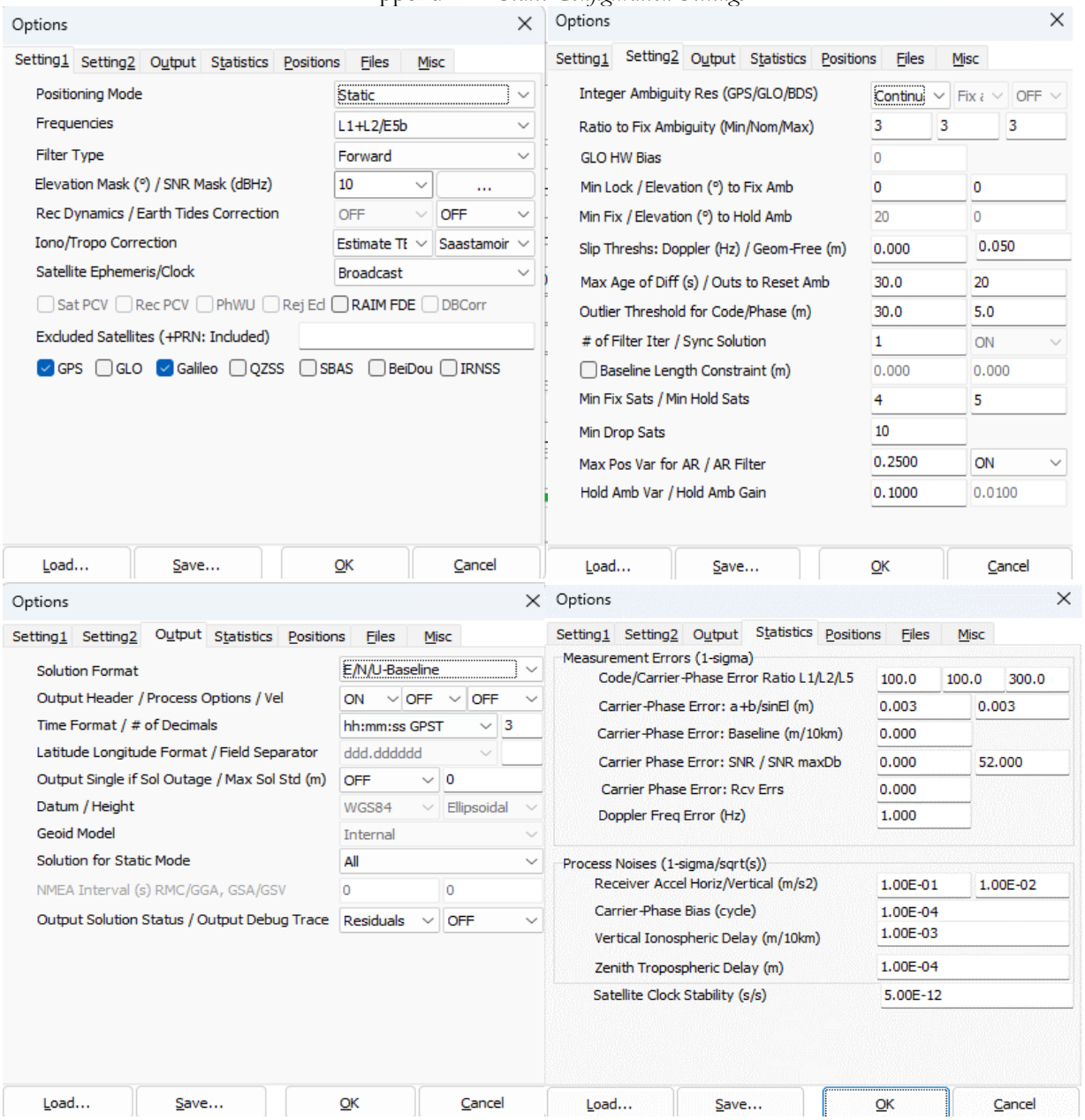

Figure D1. RTKPost configuration settings for static mode; the position file generated was used to generate estimated position reference using Excel

Appendix E: *Kinematic Configuration Settings*

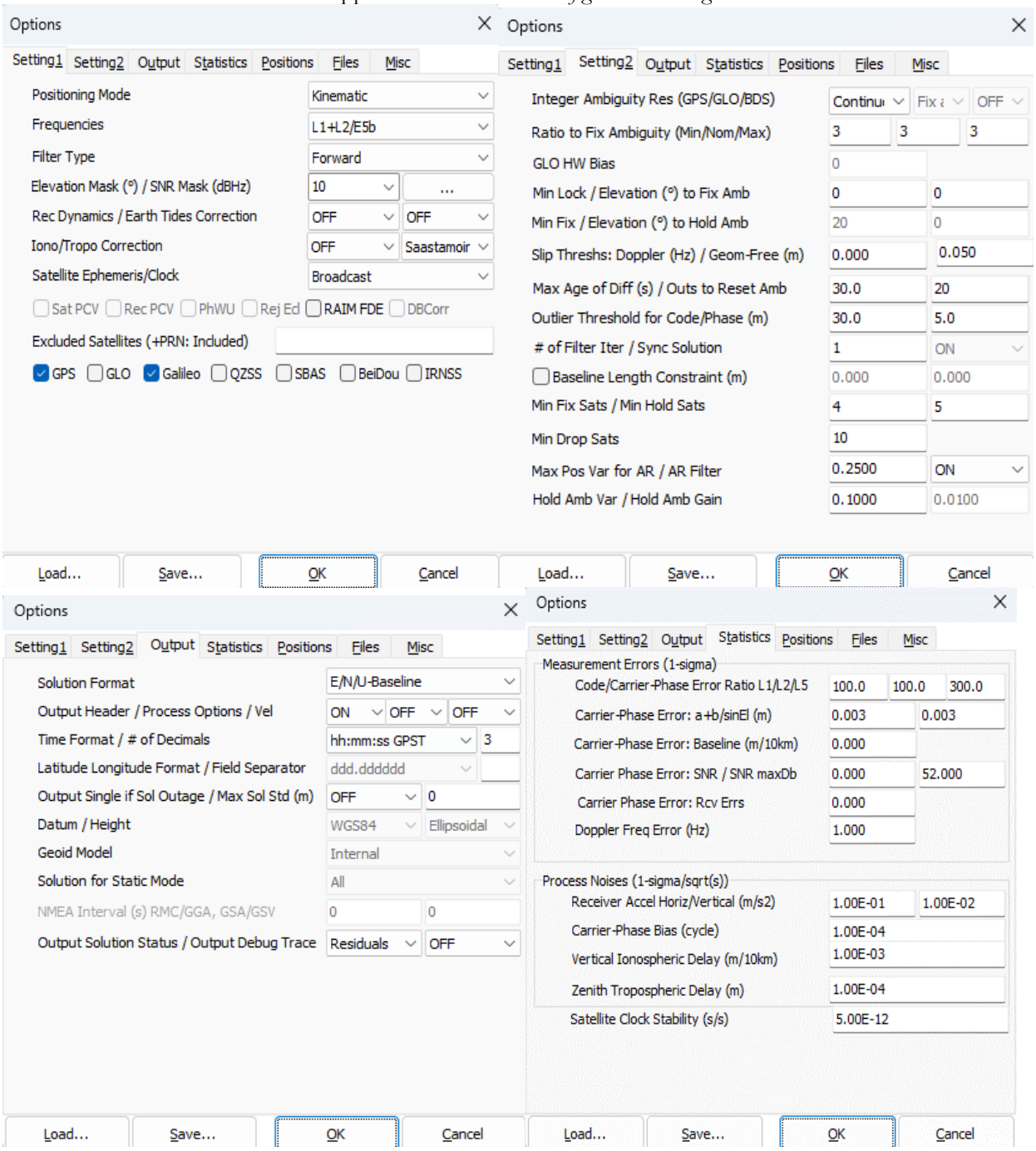

Figure E1. RTKPost configuration settings for kinematic mode. The position file generated was used to generate the 2D errors

Appendix F: *2D Error PPP 100626 on March 24*

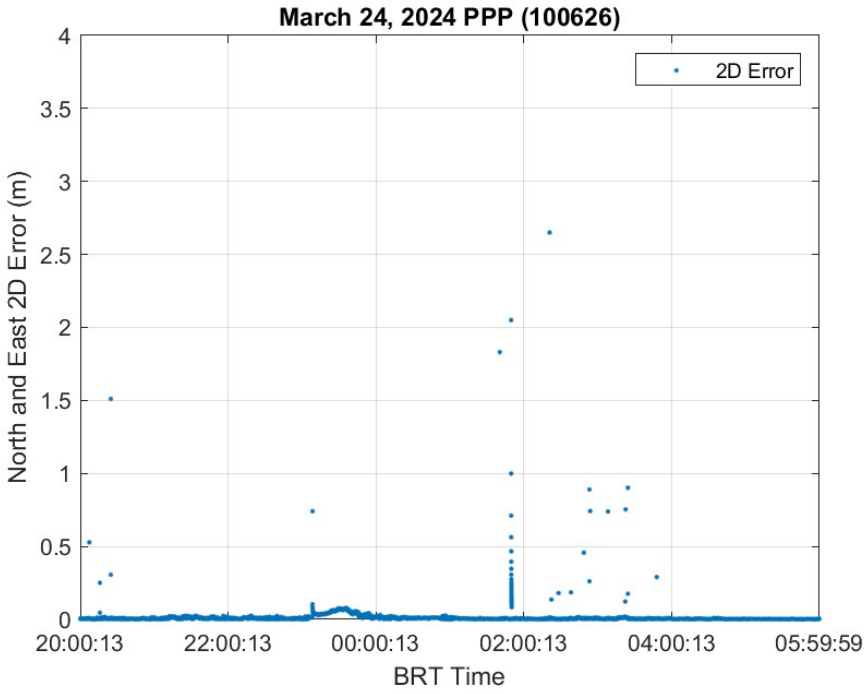

Figure F1. Scintillation impact on the 2D error of PPP 100626 on the evening of March 24

Appendix G: *Maximum S4 and sigma phi Scintillation at STMC Ground Station on March 1-2 and March 24-25, 2024*

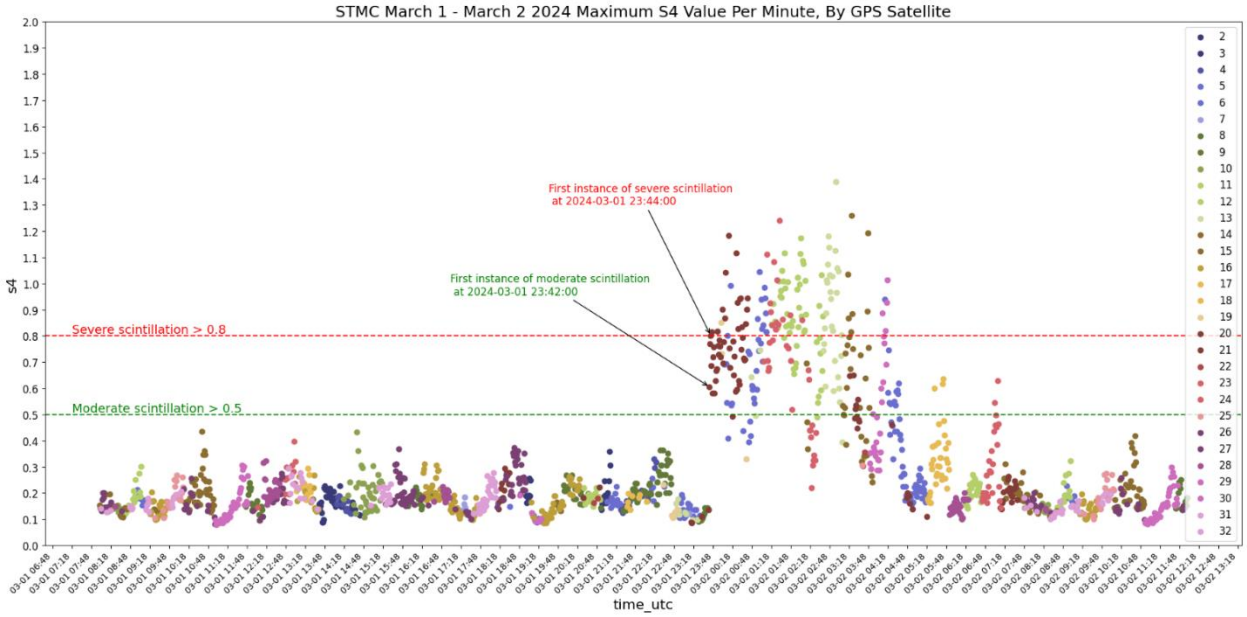

Figure G1. S4 scintillation at STMC station on the evening of March 1-2, 2024

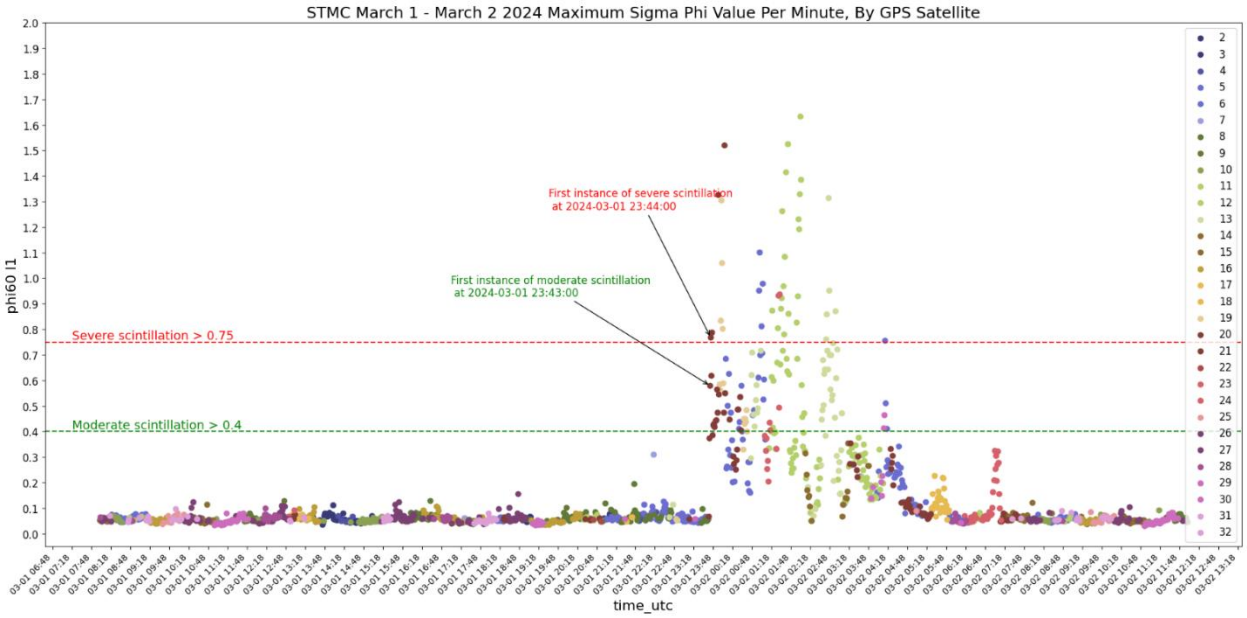

Figure G2. Sigma phi scintillation at STMC station on the evening of March 1-2, 2024

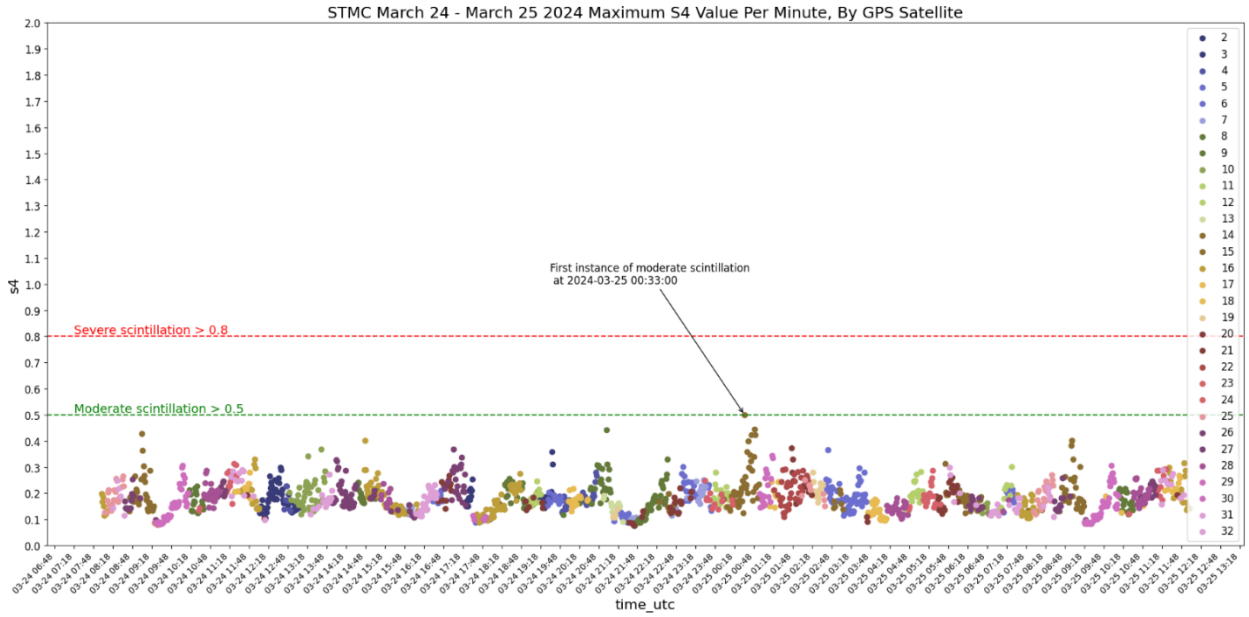

Figure G3. S4 scintillation at STMC station on the evening of March 24-25, 2024

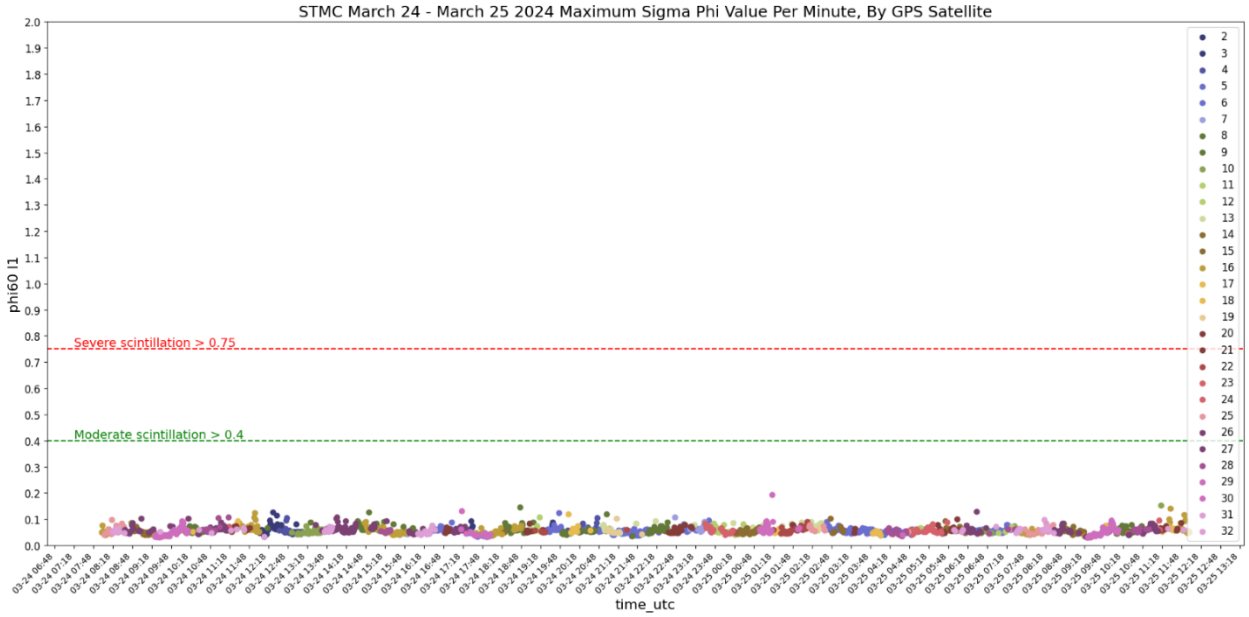

Figure G4. Sigma phi scintillation at STMC station on the evening of March 24-25, 2024

Appendix H: *March 2024 Potential Operating Windows with Maximum S4 Below Moderate Levels*

					1 Start: 01:10 AM End: 08:42 PM **Available operating time: 19 h, 32 m**	**2** Start: 04:07 AM End: 07:50 PM **Available operating time: 15 h, 43 m**
3 Start: 12:39 AM End: 11:59 PM **Available operating time: 23 h, 20 m**	**4** Start: 12:00 AM End: 08:24 PM **Available operating time: 20 h, 24 m**	**5** Start: 01:01 AM End: 08:12 PM **Available operating time: 19 h, 11 m**	**6** Start: 01:03 AM End: 08:04 PM **Available operating time: 19 h, 1 m**	**7** Start: 12:52 AM End: 08:33 PM **Available operating time: 19 h, 41 m**	**8** Start: 12:25 AM End: 08:01 PM **Available operating time: 19 h, 36 m**	**9** Start: 12:51 AM End: 10:08 PM **Available operating time: 21 h, 17 m**
10 Start: 12:19 AM End: 08:09 PM **Available operating time: 19 h, 50 m**	**11** Start: 12:15 AM End: 08:30 PM **Available operating time: 20 h, 15 m**	**12** Start: 12:32 AM End: 08:42 PM **Available operating time: 20 h, 10 m**	**13** Start: 12:13 AM End: 08:33 PM **Available operating time: 20 h, 20 m**	**14** Start: 12:09 AM End: 07:44 **Available operating time: 19 h, 35 m**	**15** Start: 01:05 AM End: 07:44 PM **Available operating time: 18 h, 39 m**	**16** Start: 01:15 AM End: 08:25 PM **Available operating time: 19 h, 10 m**
17 Start: 01:13 AM End: 08:26 PM **Available operating time: 19 h, 13 m**	**18** Start: 01:29 AM End: 07:44 PM **Available operating time: 18 h, 15 m**	**19** Start: 12:00 AM End: 09:28 PM **Available operating time: 21 h, 28 m**	**20** Start: 12:00 AM End: 10:22 PM **Available operating time: 22 h, 22 m**	**21** Start: 12:00 AM End: 11:59 PM **Available operating time: 23 h, 59 m**	**22** Start: 12:00 AM End: 08:26 PM **Available operating time: 20 h, 26 m**	**23** Start: 12:24 AM End: 08:25 PM **Available operating time: 20 h, 1 m**
24 Start: 12:00 AM End: 11:59 PM **Available operating time: 23 h, 59 m**	**25** Start: 12:00 AM End: 08:13 PM **Available operating time: 20 h, 13 m**	**26** Start: 12:45 AM End: 08:09 PM **Available operating time: 19 h, 24 m**	**27** Start: 12:00 AM End: 08:06 PM **Available operating time: 23 h, 6 m**	**28** Start: 12:00 AM End: 08:01 PM **Available operating time: 23 h, 1 m**	**29** Start: 12:46 AM End: 07:57 PM **Available operating time: 19 h, 11 m**	**30** Start: 12:12 AM End: 11:59 PM **Available operating time: 23 h, 47 m**
31 Start: 12:00 AM End: 07:48 PM **Available operating time: 19 h, 48 m**						

Figure H1. Calendar of potential operating window start times, end times, and durations for STMC station, March 2024

Appendix I: *March 2024 Potential Increase in Operating Time*

					1 + 3 h, 42 m	**2** - 0 h, 17 m
3 + 7 h, 20 m	**4** + 4 h, 24 m	**5** + 3 h, 11m	**6** + 3 h, 1 m	**7** + 3 h, 41 m	**8** + 3 h, 36 m	**9** + 5 h, 17 m
10 + 3 h, 50 m	**11** + 4 h, 15 m	**12** + 4 h, 10 m	**13** + 4 h, 20 m	**14** + 3 h, 35 m	**15** + 2 h, 39 m	**16** + 3 h, 10 m
17 + 3 h, 13 m	**18** + 2 h, 15 m	**19** + 5 h, 28 m	**20** + 6 h, 22 m	**21** + 8 h	**22** + 4h, 26 m	**23** + 4 h, 1 m
24 + 8 h	**25** + 4 h, 13 m	**26** + 3 h, 24 m	**27** + 7 h, 6 m	**28** + 7 h, 1	**29** + 3 h, 11 m	**30** + 4 h, 47 m
31 + 6 h, 48 m						

Figure I1. Differences between the potential operating window and the standard operating window for STMC station, March 2024

Appendix J: *ROTI Maps on March 1 and 24 of 2024*

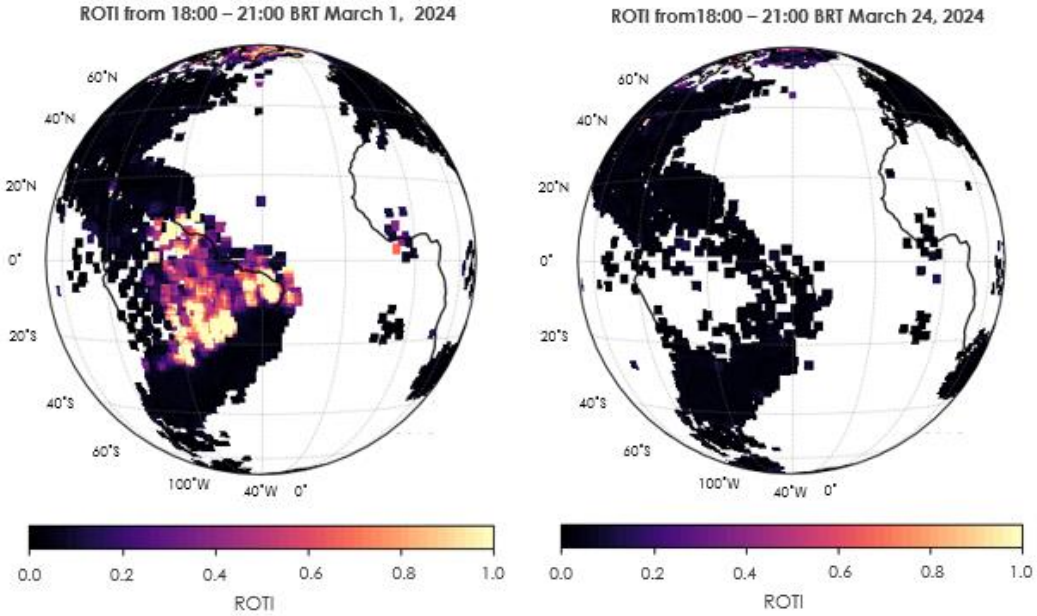

Figure J1. ROTI mappings for March 1 and 24 evenings